



Interpreting the $^{13}\text{C} / ^{12}\text{C}$ ratio of carbon dioxide in an urban airshed in the Yangtze River Delta, China

Jiaping Xu¹, Xuhui Lee^{1,2}, Wei Xiao¹, Chang Cao¹, Shoudong Liu¹, Xuefa Wen³, Jingzheng Xu¹, Zhen Zhang¹, and Jiayu Zhao¹

¹Yale-NUIST Center on Atmospheric Environment, Nanjing University of Information Science & Technology, Nanjing, China

²School of Forestry and Environmental Studies, Yale University, New Haven, Connecticut, USA

³Key Laboratory of Ecosystem Network Observation and Modeling, Institute of Geographic Sciences and Natural Resources Research, Chinese Academy of Sciences, Beijing, China

Correspondence to: Xuhui Lee (xuhui.lee@yale.edu)

Received: 23 April 2016 – Discussion started: 9 May 2016

Revised: 15 February 2017 – Accepted: 16 February 2017 – Published: 9 March 2017

Abstract. Observations of atmospheric CO_2 mole fraction and the $^{13}\text{C} / ^{12}\text{C}$ ratio (expressed as $\delta^{13}\text{C}$) in urban airsheds provide constraints on the roles of anthropogenic and natural sources and sinks in local and regional carbon cycles. In this study, we report observations of these quantities in Nanjing at hourly intervals from March 2013 to August 2015, using a laser-based optical instrument. Nanjing is the second largest city located in the highly industrialized Yangtze River Delta (YRD), eastern China. The mean CO_2 mole fraction and $\delta^{13}\text{C}$ were $(439.7 \pm 7.5) \mu\text{mol mol}^{-1}$ and $(-8.48 \pm 0.56) \text{‰}$ over this observational period. The peak monthly mean $\delta^{13}\text{C}$ (-7.44‰ , July 2013) was 0.74‰ higher than that observed at Mount Waliguan, a WMO (World Meteorological Organization) baseline site on the Tibetan Plateau and upwind of the YRD region. The highly ^{13}C -enriched signal was partly attributed to the influence of cement production in the region. By applying the Miller–Tans method to nighttime and daytime observations to represent signals from the city of Nanjing and the YRD, respectively, we showed that the $^{13}\text{C} / ^{12}\text{C}$ ratio of CO_2 sources in the Nanjing municipality was $(0.21 \pm 0.53) \text{‰}$ lower than that in the YRD. Flux partitioning calculations revealed that natural ecosystems in the YRD were a negligibly small source of atmospheric CO_2 .

1 Introduction

Atmospheric CO_2 sources and sinks in urban areas consist mainly of plant uptake and release, and fossil fuel combustion. These contributors have unique $^{13}\text{C} / ^{12}\text{C}$ ratios. City clusters are human-dominated systems with high carbon emission intensity, contributing over 70 % of the total anthropogenic CO_2 to the atmosphere (Satterthwaite, 2008). Previous urban isotopic studies emphasize carbon emissions from fossil combustion (Zondervan and Meijer, 1996; Pataki et al., 2003a; Zimnoch et al., 2004; Affek and Eiler, 2006; Newman et al., 2008). Relatively little attention is given to the $\delta^{13}\text{C}$ of carbon dioxide released by cement production, which is much higher than that of fossil fuel origin (Andres et al., 1994). Likewise, the CO_2 emitted from the burning of minerals in non-energy consumption industrial processes, such as iron and steel production, has higher $\delta^{13}\text{C}$ than that of fossil fuel (Table 2; Widory, 2006). In China, cement production and industrial processes contribute 13 % of the total anthropogenic CO_2 emission (Mu et al., 2013). Many of these industrial activities occur in or near urban areas. So far, little is known about their roles in the atmospheric carbon stable isotope budget.

One scientific motivation for quantifying the $\delta^{13}\text{C}$ of atmospheric CO_2 is that it provides constraints that allow partitioning of the net surface flux into component fluxes (Farquhar and Lloyd, 1993; Yakir and Sternberg, 2000; Pataki et al., 2003b). The ^{13}C -based partitioning method has been used primarily for vegetation ecosystems, such as forests

(Lloyd et al., 1996, 2001; Ometto et al., 2006; Zobitz et al., 2008), grasses (Ometto et al., 2002; Pataki et al., 2003b), and crops (Leavitt et al., 1995; Griffis et al., 2005). The approach has also been used in a limited number of urban studies (Pataki et al., 2003a; Zimnoch et al., 2004; Newman et al., 2008; Jasek et al., 2014). Compared with vegetation ecosystems, urban ecosystems have more complex CO_2 source configurations. We must consider both natural sources (plants and soils) and anthropogenic sources (fossil combustion and non-energy industrial processes), as well as the fact that the degree of mixing of urban air with the free troposphere and the air outside the urban boundary varies diurnally and seasonally. Anthropogenic emissions are hard to quantify because they depend on multiple factors, including city size, population density, fossil mix, and climate.

One of the first measurements of the carbon isotope ratio of CO_2 in an urban atmosphere was made by Friedman and Irsa (1967). Since then, more experiments have been conducted in urban environments (Ehleringer et al., 2002; Koerner and Klopatek, 2002; Takahashi et al., 2002; Clark-Thorne and Yapp, 2003; Lichtfouse et al., 2003; Widory and Javoy, 2003; Zimnoch et al., 2004; Bush et al., 2007; Guha and Ghosh, 2010; Wang and Pataki, 2012). The analytical technique employed in these studies is mainly based on isotope-ratio mass spectrometry (IRMS). In recent years, the development of isotope-ratio infrared spectroscopy (IRIS) and online calibration technology provides a new solution for long-term in situ observation of the CO_2 mole fraction and $\delta^{13}\text{C}$ at high frequencies (1 Hz to 1 h; Pataki et al., 2006; Griffis, 2013; Gorski et al., 2015). However, application of IRIS technology in urban monitoring is still limited in terms of cities covered and measurement duration (McManus et al., 2002; Pataki et al., 2006; Wada et al., 2011; Moore and Jacobson, 2015). Only a few published studies have presented data that span one full annual cycle (e.g., Pang et al., 2016).

Simultaneous measurement of atmospheric CO_2 concentration and $\delta^{13}\text{C}$ is used to determine the overall $^{13}\text{C}/^{12}\text{C}$ ratio of local surface sources δ_S . The majority of published urban studies to date have deployed the Keeling plot method (Keeling, 1958, 1961) for the determination of δ_S . In this approach, a linear relationship is established between $\delta^{13}\text{C}$ and the reciprocal of the CO_2 mole fraction from the observed time series, and the intercept of the linear regression is taken as the isotopic ratio of the local CO_2 emissions. The method assumes that the isotopic ratio of the sources is invariant with time. It also assumes that changes in the CO_2 mole fraction and in $\delta^{13}\text{C}$ are attributed only to the surface sources and are unaffected by regional carbon sources (Pataki et al., 2003b). However, these assumptions do not strictly hold in an urban environment because the intensity of traffic emissions varies strongly through the diel cycle (McDonald et al., 2014), and therefore the composition of the surface source varies and its $^{13}\text{C}/^{12}\text{C}$ ratio cannot be assumed constant. In addition, because of strong atmospheric mixing in the daytime convective boundary layer, the background air in the upper tro-

posphere can be easily entrained to the surface layer, mixing the CO_2 that originates from regional sources with that emitted locally in the urban airshed.

Miller and Tans (2003) propose that δ_S be determined as the slope of the linear relationship

$$\delta_a C_a - \delta_b C_b = \delta_S (C_a - C_b), \quad (1)$$

where C_a is CO_2 mole fraction in urban air, C_b is CO_2 mole fraction at a background site, δ_a is the $\delta^{13}\text{C}$ value of C_a , and δ_b is the $\delta^{13}\text{C}$ value of C_b . All the variables are time dependent. Because this approach takes into account the fact the background atmosphere varies, it may be more suitable than the Keeling method for inferring δ_S from the observations made in the urban area with complex emission sources. The method has been applied to local and regional carbon budget studies in nonurban settings (Miller et al., 2003) and in an urban environment by Newman et al. (2016). Here we extend the method to continuous measurements in an urban environment.

In this study, we report the results of long-term (30 months) continuous measurement of atmospheric CO_2 mole fraction and $\delta^{13}\text{C}$ at a suburban site in Nanjing using an IRIS instrument. Nanjing is the second largest city in the Yangtze River Delta (YRD), Eastern China, with a built-up area of 753 km^2 and a population of 8.2 million. Geographically, the YRD includes the provinces of Jiangsu, Zhejiang, and Anhui, and the Shanghai municipality (29.04 to 33.41° N , 118.33 to 122.95° E) with a population of 190 million. The YRD is influenced by subtropical moist monsoon climate. The mean annual temperature is about 15° C and the annual precipitation is between 1000 and 1800 mm. The vegetation types are all C_3 species. The YRD is the most industrialized region in China and had a higher urban land fraction of 10.8 %, as of 2014, than the global mean (2.4 %, Akbari et al., 2009). In 2014, more than 220 large cement production factories (daily output exceeding 1000 t) were located in the YRD (China Cement, 2016), contributing about 20 % of the national cement output.

The objectives of this study are (1) to characterize the atmospheric $\delta^{13}\text{C}$ diel and seasonal and annual variations in this urban environment in a region where such measurement is nonexistent; (2) to investigate the influence of cement production on atmospheric $\delta^{13}\text{C}$; (3) to evaluate the performance of the Keeling plot and the Miller–Tans methods for determining δ_S ; and (4) to explore the utility of the isotopic constraints for inferring the net surface flux and the plant CO_2 flux in Nanjing and in the YRD.

2 Methods

2.1 Atmospheric observation

An IRIS analyzer (model G1101-i, Picarro Inc., Sunnyvale, CA) was used to measure atmospheric CO_2 mole frac-

Table 1. Standard gases used for instrument calibration. The mean and standard deviation of the CO_2 mole fraction and $\delta^{13}\text{C}$ were based on six and five repeated measurements, respectively.

ID	CO_2 ($\mu\text{mol mol}^{-1}$)	$\delta^{13}\text{C}$ (‰)	Period
1 Low	381.89 ± 0.99	-29.75 ± 0.27	Mar 2013–Aug 2014
1 High	502.35 ± 0.28	-30.01 ± 0.18	Mar 2013–Aug 2014
2 Low	380.92 ± 0.95	-29.75 ± 0.27	Sep 2014–Aug 2015
2 High	501.05 ± 0.33	-30.01 ± 0.18	Sep 2014–Aug 2015

tion and $^{13}\text{C}/^{12}\text{C}$ ratio ($\delta^{13}\text{C}$) continuously from February 2013 to August 2015. The analyzer was housed on the ninth floor of our laboratory building on the campus of Nanjing University of Information, Science and Technology (NUIST, $32^\circ 12' \text{N}$, $118^\circ 43' \text{E}$), in the northern suburb of Nanjing, at a linear distance of 20 km to the city center. The instrument inlet was at a height of 34 m above the ground. There was no large industrial CO_2 source in the 3 km radius except for a commuting road located about 300 m east of the observation site. The nearest industrial complexes, the Nanjing Iron & Steel Group Co. Ltd. and the Nanjing Chemical Industry Group, were located about 5 km to the south of the site.

The measurement was made at 0.3 Hz and at an air flow rate of 30 mL min^{-1} at standard temperature and pressure. One three-way solenoid valve was combined with two two-way solenoid valves, so the analyzer could be switched for atmospheric sampling and for sampling of two standard gases. Calibration was carried out every 3 h by sampling each standard gas for 5 min following the procedure of Bowling et al., (2003) and Wen et al., (2013). To avoid transient effects, only the data collected in the last 2 min of the 5 min calibration periods were used (Fig. S1 in the Supplement). Table 1 lists the concentrations and their isotopic ratios of the standard gases used in this study. These gases were balanced in the air, and their concentration values bracketed the range of ambient concentration variability (Fig. 3). Their CO_2 mole fractions were measured with a gas analyzer (model G1301, Picarro) and calibrated against three primary standards obtained from NOAA-ESRL, which were traceable to the WMO (World Meteorological Organization) 2007 scale reported by the Central Calibration Laboratory of the World Meteorological Organization, and their $\delta^{13}\text{C}$ values were measured with a mass spectrometer (MAT-253, Finnigan) using IAEA reference materials IAEA-CO-8 (-5.76 ‰ VPDB) and IAEA-CO-9 (-47.32 ‰ VPDB). The mass spectrometer measurements of these reference materials were (-5.81 ± 0.04) and (-46.64 ± 0.08)‰. The ambient measurement was averaged to hourly intervals. The isotopic ratio was expressed in the delta notation ($\delta^{13}\text{C}$) in reference to the VPDB scale.

The typical 5 min measurement precision is 0.3‰ for $\delta^{13}\text{C}$ and $0.05 \mu\text{mol mol}^{-1}$ for CO_2 mole fraction, according to the instrument manufacturer. Our own Allan vari-

ance analysis revealed a precision of 0.05‰ for $\delta^{13}\text{C}$ and $0.07 \mu\text{mol mol}^{-1}$ for CO_2 mole fraction at the hourly averaging interval. These improvements were simply statistical, due to the increase in the number of samples being used for averaging. The precision of the ambient measurement was lower than this due to errors propagated through the calibration procedure. According to a laboratory test on an analyzer of the same model and using the same calibration procedure as ours, the hourly $\delta^{13}\text{C}$ precision is about 0.4‰ (Wen et al., 2013).

The calibration gases had much lower $\delta^{13}\text{C}$ than the ambient delta values. The mismatch in the delta value between the calibration standard and the ambient air is common in applications of the IRIS technique ($^{13}\text{C}(\text{CH}_4)$, Röckmann et al., 2016; $^{18}\text{O}(\text{H}_2\text{O})$, Lee et al., 2005; $^{13}\text{C}(\text{CO}_2)$, Bowling et al., 2003). For example, Bowling et al. (2003) used calibration standards with delta values of -29.55 and -40.58 ‰ to calibrate their optical $^{13}\text{C}(\text{CO}_2)$ instrument. But because the system measures the concentrations of the major and the minor isotopologue independently, it is not critical that the calibration standards and the measurement target have matching isotope ratios, as long as the standards bracket concentration variability of the target (Bowling et al., 2005). Nevertheless, the overall accuracy of the measurement may be further improved by using calibration standards that bracket variations in both the concentration and the delta values of ambient air samples. We could not implement this improved calibration procedure because our analyzer failed at the end of the experiment.

We did not adopt the strict filtering technique used for background sites (Thoning et al., 1989) because of high natural variations in urban airsheds. We removed the first 3 min of the data after switching to the ambient sampling mode from the calibration mode. Additionally, data were removed if the average hourly CO_2 mole fraction was lower than $390 \mu\text{mol mol}^{-1}$ (or $30 \mu\text{mol mol}^{-1}$ lower than the midafternoon value in the summer; Fig. 3) or $\delta^{13}\text{C}$ was out of the range between -15 and -5.5 ‰ (or about 3 SD from the mean); a total of 217 hourly values were removed by these outlier criteria.

The $\delta^{13}\text{C}$ value measured by the analyzer in high-humidity conditions is biased higher due to spectral broadening and direct spectral interference (Rella, 2011). To correct for the humidity interference, we carried out two tests using a dew-point generator (model 610, LI-COR, Inc., Lincoln, NE). A CO_2 standard gas (secondary standard gas, $439 \mu\text{mol mol}^{-1}$ in test one and $488 \mu\text{mol mol}^{-1}$ in test two, balanced by dry air) was fed into the dew-point generator. The outlet of the dew-point generator was connected with a three-way union with one end linked to the inlet of the analyzer and the other end open to the room. The humidity level of the air coming out of the dew point generator was regulated at eight levels in a dew-point temperature range of 1 to 30°C , giving a water vapor mole fraction ranging from 0.66 to 4.26% (0.66 to $4.26 \text{ cmol mol}^{-1}$). Measurement at each humidity

level lasted 30 min, with the first 5 min excluded from the analysis. Because the $^{13}\text{C}/^{12}\text{C}$ ratio of the standard gas was constant, any observed variations were caused by the humidity artifact. We found that no correction was needed for our analyzer if the water vapor mole fraction was below 2.03 %. Above this humidity level, the measurement was biased high by 0.46 ‰ for every 1 cmol mol^{-1} increase in the water vapor mole fraction (Fig. 1). This humidity effect is not negligible, but is an order of magnitude smaller than that reported by Rella (2011). The two tests, taken 8 months apart, yielded essentially the same result. The correction equation is

$$\delta^{13}\text{C} = \delta^{13}\text{C}_{\text{true}}, C(\text{H}_2\text{O}) \leq 2.03 \%, \quad (2a)$$

$$\delta^{13}\text{C} = \delta^{13}\text{C}_{\text{true}} + 0.46 \text{‰} (C(\text{H}_2\text{O}) \text{‰} - 2.03 \%), \\ C(\text{H}_2\text{O}) > 2.03 \%, \quad (2b)$$

where $C(\text{H}_2\text{O})$ is water vapor mole fraction and was measured by the same isotope analyzer, $\delta^{13}\text{C}$ is the measured isotope delta value (after the two-point calibration), and $\delta^{13}\text{C}_{\text{true}}$ is the true isotope delta value. The ambient vapor mole fraction varied from 0.16 to 3.64 % during the measurement period. About 35 % of the observations exceeded the threshold mole fraction of 2.03 % and required correction. The largest hourly correction was 0.74 ‰. In the following, all the data have been corrected for the humidity interference.

2.2 The $^{13}\text{C}/^{12}\text{C}$ ratio of surface sources (δ_S)

We applied the Miller–Tans method to estimate the $^{13}\text{C}/^{12}\text{C}$ ratio of the surface source (δ_S). Strictly, Eq. (1) does not allow a nonzero intercept. When applied to the urban airshed in Los Angeles, Eq. (1) does not require an intercept (Newman et al. 2016). However, when applied to the data obtained at the monthly timescale in this study, the regression yielded a nonzero intercept (Fig. S2). To determine whether a shorter timescale would improve the result, we applied the 5 h moving window technique described by Vardag et al. (2016) to the observations made in January and July 2014. Only 4 % of the data, all obtained at nighttime, satisfy their data screening criteria. The mean regression equation of this subset is $y = (-26.41 \pm 4.03)x + (428.84 \pm 211.12)$ for January and $y = (-25.64 \pm 6.39)x + (687.83 \pm 264.67)$ for July, where x is $(C_a - C_b)$ and y is $(\delta_a C_a - \delta_b C_b)$. In these analyses, the background CO_2 mole fraction and the isotope ratio were those observed at Mount Waliguan (WLG; $36^\circ 17' \text{N}$, $100^\circ 54' \text{E}$; 3816 m a.m.s.l. (above mean sea level) <https://www.esrl.noaa.gov/gmd/dv/data/index.php>) located at the northeastern edge of the Tibetan Plateau (Zhou et al., 2005), the closest upwind WMO background station for Nanjing. Use of other WMO baseline sites as the background gave essentially the same results.

The selection of a background site is a critical issue when applying the Miller–Tans method (Ballantyne et al., 2010, 2011). That the Miller–Tans intercept does not go to zero suggests that the baseline site WLG may not be a suitable

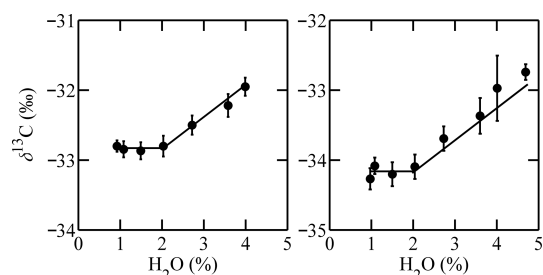


Figure 1. Dependence of the observed $\delta^{13}\text{C}$ on the H_2O mole fraction. The lines represent Eq. (2). Error bars are ± 1 SD of 1 min averages. The data in the left panel were obtained on 1 October 2014 using a $439 \mu\text{mol mol}^{-1}$ standard gas and the true $\delta^{13}\text{C}$ value of -32.8‰ , and those in the right panel on 10 June 2015 using a $488 \mu\text{mol mol}^{-1}$ standard gas and the true $\delta^{13}\text{C}$ value of -34.1‰ .

background for this highly urbanized region. We tested the Miller–Tans method with other isotope data published for urban areas, and found that the intercept was nonzero for the data obtained by Sturm et al. (2006) at Bern, Switzerland (Fig. S3), and a number of other urban datasets (Table S1 in the Supplement).

In the following, we used the tropospheric CO_2 mole ratio calculated by CarbonTracker over the YRD region (altitude 3330 m; <https://www.esrl.noaa.gov/gmd/dv/data/index.php>) as the background concentration (C_b). The CarbonTracker mole ratio is on average $3.5 \mu\text{mol mol}^{-1}$ higher than that observed at WLG. To overcome the problem that CarbonTracker does not calculate tropospheric $\delta^{13}\text{C}$, we rearranged Eq. (1) to a form that allows an intercept but without the need for a known background $\delta^{13}\text{C}$, such as

$$\delta_a C_a = \delta_S (C_a - C_b) + \delta_b C_b. \quad (3)$$

The $^{13}\text{C}/^{12}\text{C}$ ratio of the surface source was taken as the slope of the linear regression of $\delta_a C_a$ against $(C_a - C_b)$. A key difference between Eq. (3) here and Eq. (5) of Miller and Tans (2003) is that the δ_S appears only in the slope parameter in Eq. (3) but in both the slope and the intercept parameter in Miller and Tans' (2003) Eq. (5). This modified Miller–Tans analysis requires knowledge of background CO_2 mole fraction but not δ_b .

The Miller–Tans analysis was performed over monthly intervals, using the data collected in daytime hours (10:00 to 16:00 LT – local time) to represent YRD and data collected during nighttime hours (22:00–06:00 LT) to represent Nanjing. Morning and evening transitional periods were omitted to avoid the confounding effects of sign change of the biological CO_2 flux and sudden changes in the atmospheric stability regime.

We interpreted the daytime results to represent the influence of surface sources in the YRD region and the nighttime results to represent the influence of surface sources in the Nanjing municipality. The vigorous turbulent exchange in the daytime boundary layer diminishes the role of lo-

cal sources in the measured concentration and isotopic ratio. In other words, the daytime measurement has a much larger source footprint than the size of the urban land itself or the footprint of the nighttime measurement. In contrast, the buildup of CO_2 at night is primarily the result of sources in the city (Shen et al., 2014), so we considered the δ_S determined from the nighttime observations to represent the signal of the sources located in the city. Admittedly, this interpretation of daytime versus nighttime source areas is a simplification because the actual source area also depends on thermal stratification and boundary layer wind. Nevertheless, it is supported by a trajectory analysis and by an analysis of the atmospheric methane to CO_2 emissions ratio (Shen et al., 2014).

For the purpose of comparing with the Miller–Tans results, we also estimated the source $^{13}\text{C}/^{12}\text{C}$ ratio using the Keeling mixing line method. According to Wehr and Saleska (2017), for the measurement uncertainties of our instrument system, the ordinary least squares procedure has much lower bias errors of parameter estimation than the geometric mean regression. In the following, the results of both the Miller–Tans method and the Keeling mixing line method were based on the ordinary least squares regression.

2.3 Inventory of anthropogenic sources

We calculated the anthropogenic CO_2 fluxes from energy consumption and industrial process following the SCOPE 1 procedure issued by the International Council for Local Environmental Initiatives (ICLEI, 2008). The procedure considers only emissions from sources that lie within the geographic boundary of investigation. The energy consumption source consists of direct emissions from the three main energy consumption sectors (industry, transport, and household). We ignored the commerce sector here because the main energy consumption in this sector in Nanjing and in the YRD was electric power generated by coal and coal consumption, which was already considered in SCOPE 1. The amounts of CO_2 emission were estimated with the IPCC methodology adopting the emission factors for each fossil fuel type recommended by IPCC. The calculations were done separately for the YRD region and for the Nanjing municipality. Since no statistical data were available for energy consumption in the transport sector in Nanjing, the CO_2 emission from the transport sector was deduced according to vehicle number, average annual driving distance and coefficients of fuel economy (Bi et al., 2011). We obtained the data on energy consumption from official sources (CESY, 2013; CSY, 2013; NSY, 2013).

The non-energy industrial processes included cement, raw iron, crude steel, and ammonia synthesis processes. In the YRD, the data were available at monthly intervals. For the city of Nanjing, only annual statistics were available.

2.4 Partitioning the net surface flux

We partitioned the surface CO_2 flux (F_S) into three component fluxes according to the following mass conservation equations:

$$F_S = F_F + F_C + F_P, \quad (4)$$

$$\delta_S F_S = \delta_F F_F + \delta_C F_C + \delta_P F_P, \quad (5)$$

where F_F is the flux from fossil fuel combustion and industrial emission except cement production (termed “fossil plus”); F_C is the flux due to cement production; F_P is the biological flux; and δ_F , δ_C , and δ_P are the $\delta^{13}\text{C}$ value of F_F , F_C and F_P , respectively. These CO_2 mass fluxes are obtained by dividing the total emission by the surface area within the geographic boundary of Nanjing or the YRD, having dimensions of $\text{mg m}^{-2} \text{s}^{-1}$. We separated the cement source from other non-energy consumption industrial processes because its $^{13}\text{C}/^{12}\text{C}$ ratio is much higher. In these equations, the monthly net surface flux (F_S) and the biological flux (F_P) are unknowns to be solved for, and all other terms are provided either by the atmospheric measurement or by the inventory calculation. The partitioning analysis was done for both Nanjing and the YRD using the nighttime and daytime observations, respectively.

The value for δ_F was the weighted average of the isotope ratio of individual fuel types and industrial processes (Table 2). The delta value of CO_2 from cement production is provided by Anders et al. (1994). We adopt a value of (-28.2%) for δ_P for the YRD and Nanjing, on account of a linear relationship between δ_P and tree age (Fessenden and Ehleringer, 2002), a typical tree age in this region (40 years), and a U-shaped relationship between δ_P and annual precipitation (Pataki et al., 2007). Our δ_P is more negative than that reported for a boreal forest (-26.2% ; Pataki et al., 2007) but is in closer agreement with the value reported for a ginkgo tree in Nanjing (-29.3% ; Sun et al., 2003). A summary of the isotopic ratios of the four source categories is given in Table 3.

Uncertainties in the delta values of the different fuel types and industrial processes were based on the data found in the references listed in Table 2. The uncertainty in δ_P was assumed to be $\pm 1.00\%$ (Verdag et al., 2016). The mass flux terms F_F and F_C were assumed to have a 10 % uncertainty, which is typical of fossil fuel consumption data (Vardag et al., 2016).

To partition the nighttime flux for Nanjing, we assumed that the nighttime F_F was 20 % of the daily value. The parameter 20 % was determined by the diel variation of the CO_2 flux observed with an eddy covariance system in Nanjing (Bai, 2011) and in several other cities (Coutts et al., 2007; Song and Wang, 2011; Liu et al., 2012). At night, most of the factories in the city were closed and the traffic flow was reduced to about 80 % of the daytime volume (Yang et al., 2011).

Table 2. Percentage of “fossil-plus” sources and their $\delta^{13}\text{C}$ values for the YRD and Nanjing. The uncertainty in the total “fossil-plus” source is a weighted mean of the individual uncertainties.

Sources	Percentage (%)		$\delta^{13}\text{C}$ (‰)		References
	YRD	Nanjing	YRD	Nanjing	
Coal	70.0	52.3	-25.46 ± 0.39	-25.46 ± 0.39	Duan (1995), Widory and Javoy (2003)
Gasoline	2.1	11.4	-28.69 ± 0.50	-28.69 ± 0.50	Widory and Javoy (2003)
Diesel	3.2	1.6	-28.93 ± 0.26	-28.93 ± 0.26	Widory (2006)
Fuel oil	2.1	0.3	-29.32 ± 0.15	-29.32 ± 0.15	Widory and Javoy (2003)
Natural gas	2.7	5.0	-39.06 ± 1.07	-39.06 ± 1.07	Widory and Javoy (2003)
LPG	0.7	0.2	-31.70 ± 0.40	-31.70 ± 0.40	Widory (2006)
Pig iron	8.7	12.7	-24.90 ± 0.40	-24.90 ± 0.40	Pan (2007)
Crude steel	1.5	0.7	-25.28 ± 0.40	-25.28 ± 0.40	Wang (2013)
Ammonia synthesis	9.0	15.9	-28.18 ± 0.55	-28.18 ± 0.55	An (2012)
Total	100	100	-26.36 ± 0.42	-26.97 ± 0.46	

Table 3. Inventory data for the isotopic composition of surface CO_2 sources and their percentage of contribution in the YRD and in Nanjing. Here the “fossil-plus” category includes all non-cement anthropogenic emissions listed in Table 2. The cement isotopic ratio is based on Andres et al. (1994). The approximate range in the biological isotope ratio is based on Vardag et al. (2016).

Sources	YRD		Nanjing	
	$\delta^{13}\text{C}$ (‰)	Percentage (%)	$\delta^{13}\text{C}$ (‰)	Percentage (%)
“Fossil-plus”	-26.36 ± 0.42	91.0	-26.97 ± 0.46	96.4
Cement	0 ± 0.30	9.0	0 ± 0.30	3.6
Anthropogenic	-23.99 ± 0.41	100	-26.00 ± 0.45	100
Biological	-28.20 ± 1.00	–	-28.20 ± 1.00	–

The partitioning equations are explicit expressions of the mass balance principle. But uncertainties in the isotope delta end members and the anthropogenic fluxes can propagate through these equations, causing uncertainties in the estimation of F_S and F_P . Here we used a Monte Carlo analysis to quantify the error propagation. The same analysis has been applied to the partitioning of lake water budgets from isotope end members (Jasechko et al., 2014). The procedure employed a Gaussian distribution for errors in the input variables and an ensemble of 10 000 realizations for each month. Errors in F_S and F_P were computed as 1 standard deviation of these realizations after excluding the top and bottom 50 extreme ensemble members.

3 Results

3.1 Temporal variations in the CO_2 mole fraction and $\delta^{13}\text{C}$

The monthly CO_2 mole fraction during the summer was slightly lower than in the other seasons (Fig. 2). The mean mole fraction was 446.7 and $431.1 \mu\text{mol mol}^{-1}$ for January and July, respectively, giving a seasonal amplitude of

$15.6 \mu\text{mol mol}^{-1}$. The mean CO_2 mole fraction during the whole experimental period (March 2013 to August 2015) was $439.7 \mu\text{mol mol}^{-1}$, which is $40.6 \mu\text{mol mol}^{-1}$ higher than the value observed at WLG for the same period. In 2014, the calendar year with complete data coverage, the mean CO_2 mole fraction was $441.2 \mu\text{mol mol}^{-1}$, which is 42.5 ppm higher than the WLG value for the same year.

The $^{13}\text{C} / ^{12}\text{C}$ ratio of atmospheric CO_2 displayed a more clear seasonal cycle than the mole fraction (Fig. 2). The monthly mean value was $(-9.07 \pm 0.17) \text{‰}$ (mean \pm standard error) and $(-7.63 \pm 0.18) \text{‰}$ for January and July, respectively, with a seasonal amplitude of 1.44‰ . The mean value for the whole experimental period was -8.48‰ , which is the same as the WLG value (-8.48‰). The summertime (June to August) $\delta^{13}\text{C}$ was 0.39‰ higher than the WLG background value. The seasonality of the $^{13}\text{C} / ^{12}\text{C}$ ratio at Nanjing was greater than that at WLG.

The strongest diel variation in the CO_2 mole fraction was observed in the autumn season (September to November) and the weakest in the winter season (December to February), with a diel amplitude of 27.9 and $13.4 \mu\text{mol mol}^{-1}$, respectively (Fig. 3). In the summer season, the peak value was observed at 07:00 LT and the lowest value at 19:00 LT. In contrast to the CO_2 mole fraction, $\delta^{13}\text{C}$ showed the lowest value

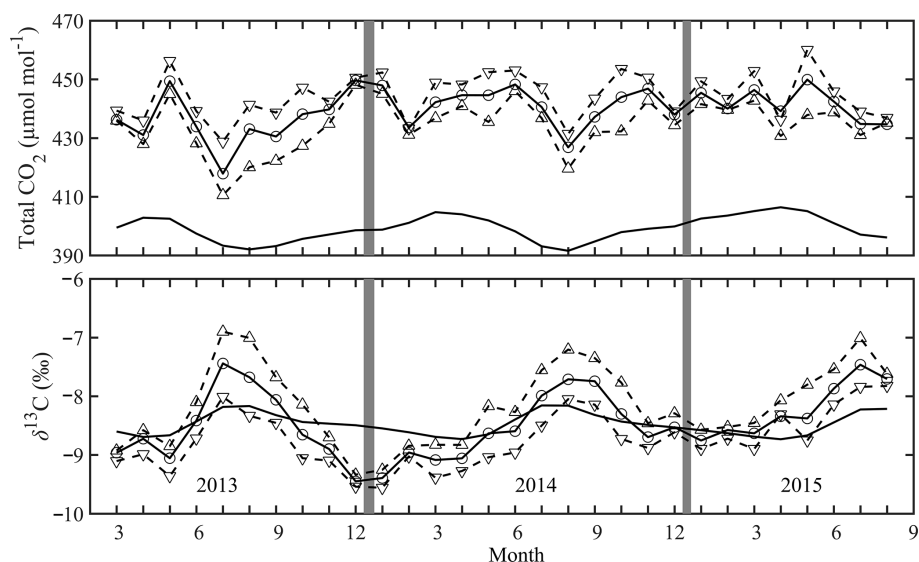


Figure 2. Monthly total CO_2 mole fraction (upper panel) and $\delta^{13}\text{C}$ (lower panel): solid lines with circles are whole-day means; dashed lines with up triangles represent daytime (10:00–16:00 LT) means; dashed line with down triangles (∇ = downward triangle, \triangle = upward triangle) represent nighttime (22:00–06:00 LT) means; smooth solid lines are monthly means observed at WLG.

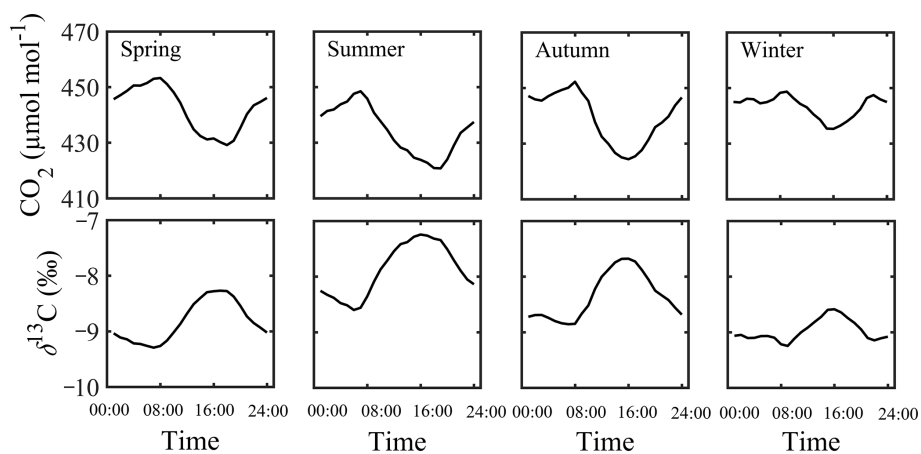


Figure 3. Mean diel variation of the CO_2 mole fraction (upper panels) and the $\delta^{13}\text{C}$ value (bottom panels) between March 2013 and August 2015.

in the early morning and the highest value in the afternoon in all the four seasons. The diel amplitude was 1.36‰ in the summer and 0.66‰ in the winter.

3.2 $^{13}\text{C}/^{12}\text{C}$ ratio of the surface sources (δ_S)

Figures 4 and 5 show an example of the modified Miller–Tans approach applied to the month of January 2014. According to the slope parameter estimation, the $^{13}\text{C}/^{12}\text{C}$ ratio of the surface sources was $(-25.01 \pm 0.90)\text{‰}$ (mean $\pm 95\%$ confidence limit for the YRD (Fig. 4) and $(-25.23 \pm 0.74)\text{‰}$ for Nanjing (Fig. 5).

Figure 6 shows the monthly isotopic ratio calculated with the Miller–Tans method for the whole observation period. The reader is reminded here that the results obtained for the daytime and the nighttime period represent sources in the YRD and in Nanjing, respectively. During the 2.5 years of observation, the monthly δ_S for the YRD was lower in the winter ($(-24.37 \pm 0.71)\text{‰}$) and higher in the summer ($(-23.42 \pm 1.79)\text{‰}$). The seasonal difference for Nanjing was smaller than for the YRD ($(-24.87 \pm 0.51)\text{‰}$) in the winter (December to February) and $(-24.80 \pm 1.79)\text{‰}$ in the summer months (June to August). The sources in the YRD had slightly higher δ_S than those in Nanjing. The mean δ_S value of the whole observational period was (-24.37 ± 0.61) and $(-24.58 \pm 0.44)\text{‰}$ for the YRD

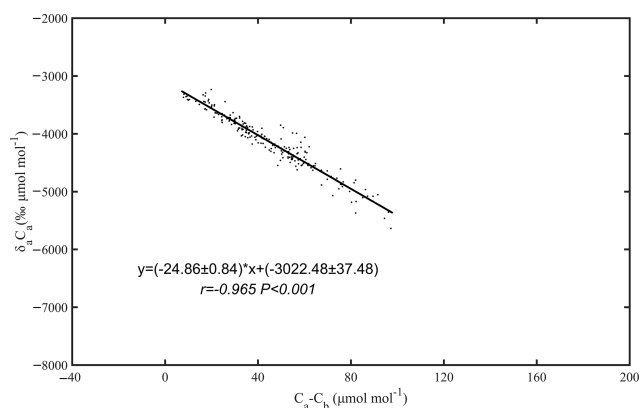


Figure 4. Application of the Miller–Tans method to the daytime (10:00–16:00 LT) data obtained in January 2014. Each data point is a 1-hourly mean. The solid line is the least squares regression according to Eq. (3). Errors bounds on the regression coefficients are at 95 % confidence intervals.

and Nanjing, respectively. The monthly δ_S for the YRD (Fig. 6a) was highly correlated with the monthly atmospheric $\delta^{13}\text{C}$ (Fig. 2; $\delta_S = (2.29 \pm 0.78) \delta^{13}\text{C} + (-5.71 \pm 6.37)$, linear correlation coefficient = 0.47, $n = 30$, $p < 0.01$). The correlation between the monthly δ_S for Nanjing (Fig. 6b) and the monthly atmospheric $\delta^{13}\text{C}$ was weak ($\delta_S = (2.39 \pm 0.92) \delta^{13}\text{C} + (-3.71 \pm 8.07)$, linear correlation coefficient = 0.03, $n = 30$, $p = 0.87$). These correlation patterns suggest that atmospheric $\delta^{13}\text{C}$ was influenced more by surface sources at the regional scale than at the local (city) scale.

3.3 Inventory data for anthropogenic sources

The emission strength of anthropogenic sources and their $^{13}\text{C}/^{12}\text{C}$ ratios were calculated with the inventory method and the data found in the literature, as described in Sect. 2.3. In the YRD, coal combustion was by far the largest source of anthropogenic CO_2 , contributing 70 % of the overall “fossil-plus” emission (Table 2). Here the “fossil-plus” emission includes contributions from all forms of fossil fuel combustion and from non-cement industrial processes. The second and third largest source were ammonia synthesis and pig iron manufacturing, with fractional contributions of about 9 %. The “fossil-plus” source contribution to the total anthropogenic emission was 91 %, with the remaining 9 % contributed by cement production (Table 2).

In the Nanjing municipality, the fractional contribution of coal to the “fossil-plus” total was 52 %, lower than that for the YRD, and the other three major sources were ammonia synthesis (16 %), pig iron (13 %), and gasoline (11 %). The fractional contribution of fossil-plus sources to the total anthropogenic emission was 96.4 % and the fractional contribution of cement production was 3.6 % (Table 2). The iso-

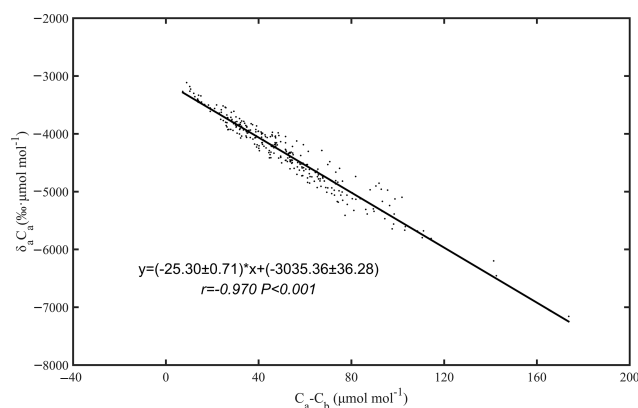


Figure 5. Same as Fig. 4 but for nighttime (22:00–06:00 LT) data obtained in January 2014.

topic ratio of the “fossil-plus” sources was 0.35 ‰ lower for Nanjing than for the YRD.

The overall effective isotopic ratio of the anthropogenic sources weighted by the source contributions was also lower for Nanjing than for the YRD (Table 3). The difference was 1.76 ‰ and was a result of lower fractional contributions of coal combustion and cement production in Nanjing, which have relatively high ^{13}C contents, and a higher fractional contribution of natural gas, which is the fuel type with the lowest ^{13}C content.

3.4 CO_2 fluxes in YRD and Nanjing

Figure 7 shows the biological flux F_P and surface flux F_S calculated from the mass balance and the cement flux F_C and “fossil-plus” F_F . The F_P flux obtained with the isotopic partitioning method for the YRD agreed with the seasonal phenology expected for plants in this region. It was near zero or slightly negative in the summer and generally positive in the winter, indicating uptake and release, respectively. The annual mean daytime biological flux was $(0.03 \pm 0.64) \text{mg m}^{-2} \text{s}^{-1}$ in the YRD in the calendar year 2014. The net surface flux F_S was $(0.17 \pm 2.02) \text{mg m}^{-2} \text{s}^{-1}$ in 2014. The standard deviations of these estimates are quite large. If the extreme standard deviations of F_P ($5.16 \text{mg m}^{-2} \text{s}^{-1}$) and F_S ($22.00 \text{mg m}^{-2} \text{s}^{-1}$) in March 2014 were excluded, the mean standard deviation of F_P would decrease to $0.23 \text{mg m}^{-2} \text{s}^{-1}$ and to that of F_S to $0.20 \text{mg m}^{-2} \text{s}^{-1}$.

In Nanjing, the biological flux was positive throughout the year (Fig. 8). This is because the partitioning was done for the night hours, when the natural ecosystems were a source of CO_2 due to autotrophic and heterotrophic respiration. The annual mean nighttime biological flux for the calendar year 2014 was $(0.06 \pm 0.26) \text{mg m}^{-2} \text{s}^{-1}$. The nighttime surface flux was $(0.18 \pm 0.22) \text{mg m}^{-2} \text{s}^{-1}$ in 2014.

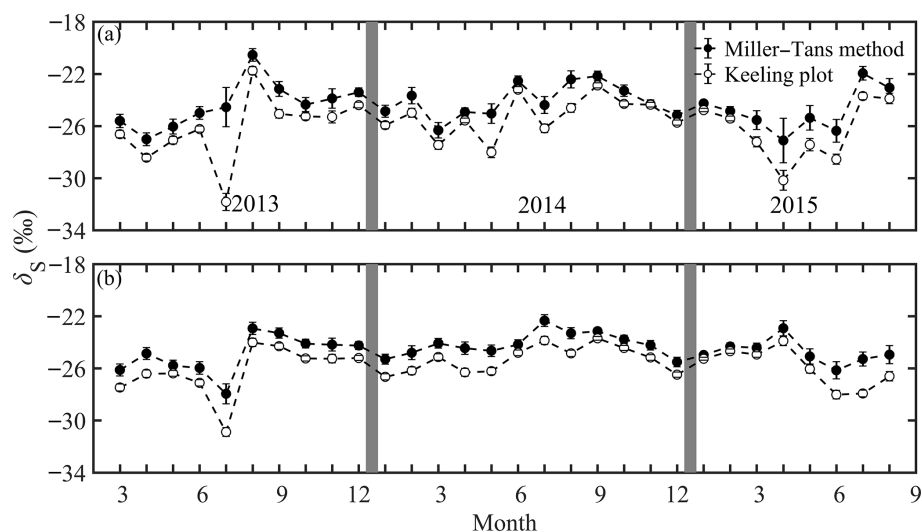


Figure 6. Time series of monthly $^{13}\text{C}/^{12}\text{C}$ ratio of surface sources in the YRD (a) and in Nanjing (b), obtained from daytime and nighttime measurement, respectively. The error bars are ± 1 SD of the regression coefficient.

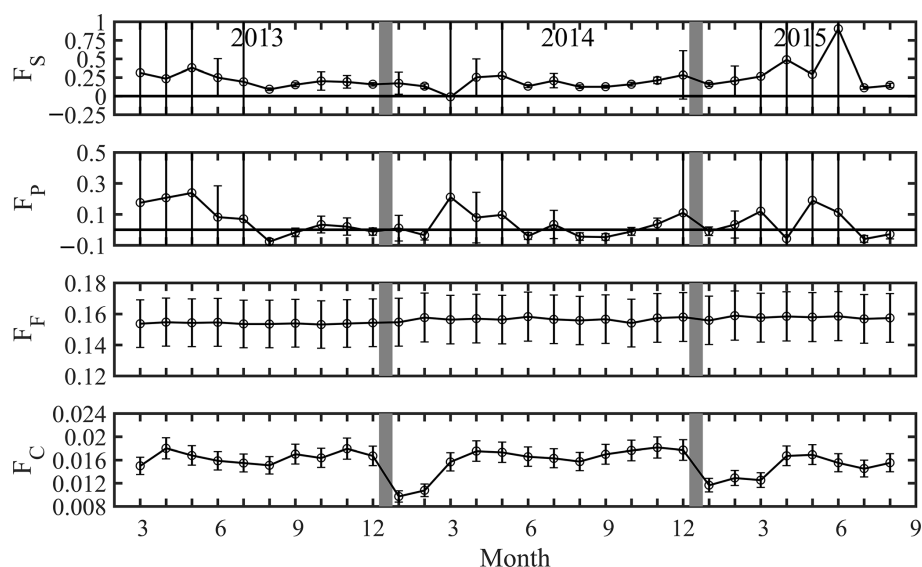


Figure 7. Time series of monthly net surface CO₂ flux (F_S), biological CO₂ flux (F_P), anthropogenic CO₂ flux excluding cement emission (F_F), and cement CO₂ flux (F_C) in the YRD. All the CO₂ mass fluxes are in $\text{mg m}^{-2} \text{s}^{-1}$. The flux terms F_F and F_C are assumed to have a 10% uncertainty typical of fossil fuel consumption data. The partitioning results (F_P and F_S) are based on the source $^{13}\text{C}/^{12}\text{C}$ ratio derived from daytime atmospheric measurements.

4 Discussion

4.1 CO₂ mole fraction and $\delta^{13}\text{C}$ seasonality

The atmospheric CO₂ mole fraction observed in Nanjing showed very small seasonal variation (a summer versus winter difference of $7.9 \mu\text{mol mol}^{-1}$, a July versus January difference of $15.6 \mu\text{mol mol}^{-1}$), in comparison with the data published for other cities. For example, in Salt Lake City, USA, the CO₂ mole fraction in the summer is about $31 \mu\text{mol mol}^{-1}$ lower than in the winter (Pataki et al., 2003a). Several factors

contributed to the weak seasonality in Nanjing. The climate in the YRD is relatively mild. The governmental energy policy prohibits winter heating in public buildings. Most residential buildings also lack space heating in the winter. This is in contrast to energy use patterns in northern cities in China and elsewhere. The weak seasonality of the observed mole fraction was also related to the low vegetation cover in the YRD and in Nanjing. The forest cover ratio is about 35% in Nanjing and in the YRD, and the overall vegetation cover (forest plus other vegetation types) ratio in the major cities

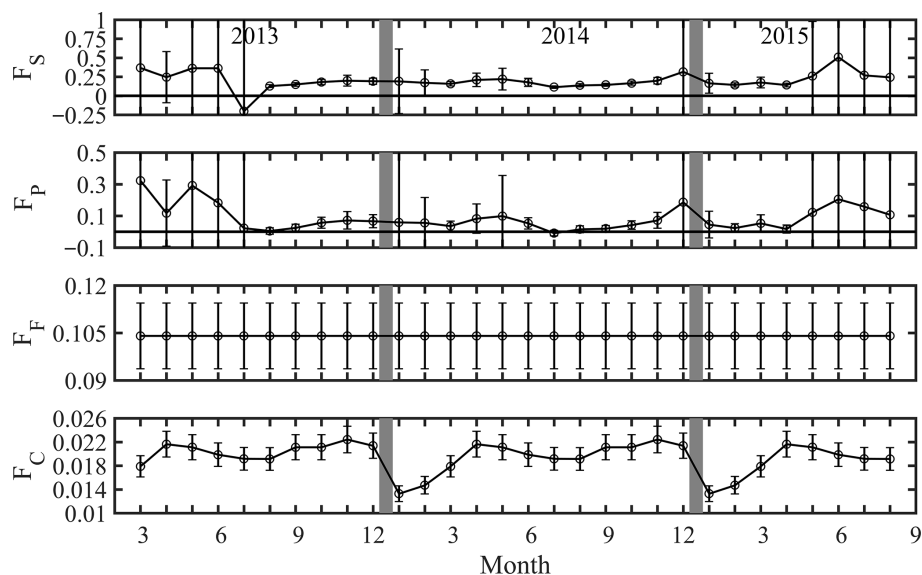


Figure 8. Time series of monthly net surface CO_2 flux (F_S), biological CO_2 flux (F_P), anthropogenic CO_2 flux excluding cement emission (F_F), and cement CO_2 flux (F_C) in Nanjing. All the CO_2 mass fluxes are in $\text{mg m}^{-2} \text{s}^{-1}$. The flux terms F_F and F_C are assumed to have a 10 % uncertainty typical of fossil fuel consumption data. The partitioning results (F_P and F_S) are based on the source $^{13}\text{C}/^{12}\text{C}$ ratio derived from nighttime atmospheric measurements.

in the YRD is lower than 45 % (CESY, 2013; CSY, 2013). In comparison, the vegetation cover ratio is 56 % in Salt Lake City (Pataki et al., 2009) and 44 % in Chicago (Rose et al., 2003). Dense vegetation is known to deplete atmospheric CO_2 in the summer season via photosynthetic uptake, amplifying the CO_2 seasonal amplitude.

Our $\delta^{13}\text{C}$ seasonal amplitude (January vs. July difference of 1.44 ‰) was 4 times the amplitude observed or estimated at WLG (Fig. 2) but agreed with those reported by most urban studies. In comparison, the seasonal amplitude of $\delta^{13}\text{C}_a$ in Bangalore, India, was 0.89 to 1.32 ‰ (Guha and Ghosh, 2015). Similar amplitudes have also been reported for Chicago (January versus August difference of 1.25 ‰; Moore and Jacobson, 2015) and Beijing (2.13 ‰; Pang et al., 2016). In Salt Lake City, the seasonal amplitude of $\delta^{13}\text{C}$ was approximately 1.6 ‰ because of much more natural gas consumption for heating in the winter than in the summer (Pataki et al., 2006).

4.2 Influences of cement production on atmospheric $\delta^{13}\text{C}$

The high summer $\delta^{13}\text{C}$ was one of the most unique characteristics at our site. The daytime $\delta^{13}\text{C}$ reached -6.90 ‰ in July 2013 and -7.21 ‰ in August 2014, which were 1.28 and 0.95 ‰ higher than the WLG values. The highest monthly mean $\delta^{13}\text{C}$ occurred in July: -7.44 ‰ in July 2013, -7.99 ‰ in July 2014 and -7.46 ‰ in July 2015. These values were 0.74, 0.16, and 0.77 ‰ higher than the WLG value reported for the same months.

The high July values observed at our site cannot be fully explained by CO_2 removal by plant photosynthesis. Photosynthesis and respiration are the two processes that dominate the $^{13}\text{C}/^{12}\text{C}$ seasonality in plant-dominated landscapes, leading to higher $\delta^{13}\text{C}$ values in the summer and lower values in the winter. For example, in Park Falls, Wisconsin, USA, a site in a heavily forested landscape, $\delta^{13}\text{C}$ was -7.75 ‰ in August 2011 and -8.77 ‰ in February 2012 (Moore and Jacobson, 2015). In comparison, $\delta^{13}\text{C}$ was -8.24 and -8.38 ‰ at the Mauna Loa Observatory and -8.02 and -8.66 ‰ at WLG in these 2 months, respectively. In other words, the photosynthetic effect raised the August $\delta^{13}\text{C}$ by 0.5 ‰ above the background value, a smaller enrichment than observed at our site. Due to the low vegetation fraction, the summer photosynthetic CO_2 uptake in the YRD and in Nanjing should be lower than at Park Falls. According to the CarbonTracker inversion analysis (Peters et al., 2007), the net ecosystem production at the grid point where Parks Fall is located is $-0.201 \text{ mg m}^{-2} \text{ s}^{-1}$ in July 2014 but is only $-0.059 \text{ mg m}^{-2} \text{ s}^{-1}$ at the grid point corresponding to the YRD region. We would expect from the photosynthetic effect alone that the summertime ^{13}C enrichment at our site would be smaller, not greater than that observed at Park Falls.

Furthermore, in a human-dominated landscape, the plant photosynthetic enhancement of ^{13}C is offset by the CO_2 from fossil fuel combustion, which has lower $^{13}\text{C}/^{12}\text{C}$ ratios than the atmosphere. In Chicago, the monthly mean $\delta^{13}\text{C}$ peaked in August at -8.29 ‰ during the calendar year 2011, which is 0.05 ‰ lower than the WLG value for the same month. Similarly, in Beijing, the monthly mean $\delta^{13}\text{C}$ peaked

at -9.49% in August 2014, which is 1.23% lower than the WLG value for the same month.

We suggest that cement production was the contributing factor responsible for the high $\delta^{13}\text{C}$ values in the summer. The evidence supporting this interpretation is provided by data in Table 3 and Fig. 7. The delta value of anthropogenic CO_2 in the YRD would be $-26.36 \pm 0.42\%$ without cement production and increased to $-23.95 \pm 0.41\%$ after inclusion of the cement source (Table 3). This value is much higher than those reported for other urban lands, such as -30.7% for Los Angeles, USA (Newman et al., 2008) and about -31% for Salt Lake City, USA (Bush et al. 2007). The overall surface source $^{13}\text{C}/^{12}\text{C}$ ratio derived from atmospheric measurements (-24.37 and -24.58% for the YRD and Nanjing, respectively; see Fig. 6) was also more enriched than those obtained from atmospheric measurements in other cities, such as $-28.1 \pm 0.8\%$ for Chicago in August and September (Moore and Jacobson, 2015), -32.4 to -27.4% for Salt Lake City in the growing season (Pataki et al., 2003a), -27.0% for Beijing in the winter heating season (Pang et al., 2016), and -29.3% for Los Angeles, USA (Newman et al., 2008).

The influence of cement production on atmospheric $\delta^{13}\text{C}$ has also been suggested for at least two other urban sites. In Bangalore, India, $\delta^{13}\text{C}$ is 0.05% higher than that observed at an island station in the Indian Ocean, and cement production in southern India is offered as a reason to explain the enrichment of urban $\delta^{13}\text{C}$ (Guha and Ghosh, 2015). The other urban site is Beijing, China, where the $\delta^{13}\text{C}$ measurement may have been influenced by cement factories outside of the city (Ren et al., 2015; Pang et al., 2016).

4.3 Net surface and biological fluxes in the YRD

As a human-dominated landscape, the YRD was a net source of CO_2 on the monthly scale even in the growing season (F_S , Fig. 7). The seasonal trends of the net surface flux F_S and the biological flux F_P were highly correlated with each other ($R^2 = 0.88$ after exclusion of three extreme outliers) because the anthropogenic source strengths were almost constant. The mean F_S between March 2013 and February 2015 was $0.19 \pm 1.16 \text{ mg m}^{-2} \text{ s}^{-1}$, which consisted of $0.15 \pm 0.02 \text{ mg m}^{-2} \text{ s}^{-1}$ from fossil combustion and industrial processes ($0.02 \pm 0.002 \text{ mg m}^{-2} \text{ s}^{-1}$ from cement production and $0.05 \pm 1.31 \text{ mg m}^{-2} \text{ s}^{-1}$ from biological activities). The total anthropogenic CO_2 flux was $0.17 \pm 0.02 \text{ mg m}^{-2} \text{ s}^{-1}$ in the YRD, a 70% increase from the value of $0.10 \text{ mg m}^{-2} \text{ s}^{-1}$ reported for 2009 (Shen et al., 2014). From 2009 to 2012, the GDP increased by 56% according to the National Statistic Yearbook.

For comparison, we extracted the flux data from the CarbonTracker database for the 6 by 6 pixels that cover the YRD region. The results show that the mean daytime (11:00 to 17:00 LT) biological flux is slightly negative at $-0.01 \text{ mg m}^{-2} \text{ s}^{-1}$ for 2014 (Peter et al., 2007). Our estimate

of F_P for 2014 was $0.03 \pm 0.64 \text{ mg m}^{-2} \text{ s}^{-1}$. As pointed out earlier, the F_P value for March 2014 was highly uncertain ($(0.21 \pm 5.16) \text{ mg m}^{-2} \text{ s}^{-1}$). If we replace this value by the mean value of February and April 2014, the 2014 mean F_P would be reduced to $0.02 \pm 0.22 \text{ mg m}^{-2} \text{ s}^{-1}$.

A source of uncertainty in our flux partitioning analysis is related to human breath (Affek and Eiler, 2006). Using the method of Prairie and Duarte (2007), we estimated that human respiration flux was 0.006 and $0.013 \text{ mg m}^{-2} \text{ s}^{-1}$, or 3.7 and 11.65% of anthropogenic emission in the YRD and in Nanjing, respectively. The food diet in the region is predominantly C_3 grains. By including this additional source in Eqs. (3) and (4) and by assuming that the isotopic ratio of digestion is the same as δ_P shown in Table 3, F_S and F_P would increase by 0.008 and $0.001 \text{ mg m}^{-2} \text{ s}^{-1}$ in the YRD and by 0.018 and $0.005 \text{ mg m}^{-2} \text{ s}^{-1}$ in Nanjing, respectively.

4.4 Comparison of the Miller–Tans and the Keeling methods

By applying the Miller–Tans method to daytime and nighttime observations separately, we obtained the effective source ratios that are consistent with the inventory analysis for the YRD and for the Nanjing municipality. The daytime measurement (solid circles in Fig. 6a) revealed that the $^{13}\text{C}/^{12}\text{C}$ ratio of all of the sources (anthropogenic and biological) was on average 0.21% higher than that obtained with the nighttime measurement (solid circles in Fig. 6b), although the difference is not statistically significant ($p = 0.38$). In comparison, the overall δ_S of the anthropogenic sources in the YRD was also higher than that in Nanjing, the difference being 2.01% (Table 3). The interpretation that the daytime observations capture the influence of surface sources in the YRD region is supported by a trajectory analysis and by an analysis of the atmospheric methane– CO_2 emissions ratio observed at the same site (Shen et al., 2014). We note that the atmospheric measurements gave a smaller difference between the YRD and Nanjing than that obtained by the inventory data, likely because of different biological contributions between the two spatial scales.

One open question with regard to the modified Miller–Tans method is what constitutes the true background air for the YRD. In this study, the background was assumed to be the tropospheric air above the YRD. The background delta value (δ_b) backed out from the intercepts shown in Figs. 4 and 5 is -7.6% , which is higher than expected, suggesting that the true background concentration C_b may be higher than the tropospheric value. One noteworthy feature about Eq. (3) is that its slope parameter is not sensitive to C_b , but its intercept parameter is. By increasing C_b by $15 \mu\text{mol mol}^{-1}$, the slope of the regression in Fig. 5 would remain unchanged, but the δ_b backed out from the new intercept value would become more reasonable (-8.23%). In Newman et al. (2016), the background air was measured at a coastal location upwind of the Los Angeles airshed. It is recommended that a

similar strategy should be used in future experiments, where simultaneous measurement is made at the coast of the East China Sea and only data collected in easterly winds are selected for the Miller–Tans analysis.

We also calculated the $^{13}\text{C}/^{12}\text{C}$ ratio of the surface sources with the Keeling plot method. Using the daytime data, the Keeling result was lower and more variable than that inferred from the Miller–Tans method using the daytime data (Fig. 6a). The two methods differed by an average of -1.51‰ (Table S2).

In comparison, the Keeling plot method showed reasonably good performance when applied to the nighttime observations. This is because surface inversion conditions effectively prevented mixing of the free-atmospheric air with the surface air, so that the single-source assumption implicit in the Keeling plot method could be satisfied. When we applied the Keeling plot method at monthly intervals to the nighttime data, the resulting δS showed very similar month-to-month variations with the value obtained with the application of the Miller–Tans method to the nighttime observations (Fig. 6b). The two methods differed by an average of 1.21‰ (Table S2).

When the δS derived from the Keeling plot method was used for flux partitioning, the results were much more erratic than shown in Figs. 7 and 8 (Figs. S4 and S5). The uncertainty ranges of the monthly F_{P} and F_{S} were 2–3 times larger. The biological flux F_{P} for the YRD was out of range for 4 months, and did not display an obvious seasonal pattern (Fig. S4). These results support our choice of the modified Miller–Tans method as the preferred approach for inferring the overall $^{13}\text{C}/^{12}\text{C}$ ratio of the surface sources in this study.

5 Conclusions

We showed that the temporal changes of $\delta^{13}\text{C}$ followed the seasonal patterns of anthropogenic and biologic CO_2 emissions, with lower values in the winter than in the summer. An unusual feature that has not been seen in other urban environments is that the $\delta^{13}\text{C}$ exceeded that of the background atmosphere in some of the summer months. The highest monthly $\delta^{13}\text{C}$ was -7.44‰ observed in July 2013, which was 0.74‰ greater than the WLG value for the same month. Evidence points to cement production as the key reason for why the atmospheric $\delta^{13}\text{C}$ was higher than at the background site. In contrast to the isotope ratio, the CO_2 mole fraction displayed very weak seasonality (July to January difference $15.6\text{ }\mu\text{mol mol}^{-1}$).

We hypothesized that the Miller–Tans method applied to the daytime and nighttime observations should yield the effective $^{13}\text{C}/^{12}\text{C}$ ratio of surface sources at the regional (YRD) and the local (Nanjing) scale, respectively. According to the results of the modified Miller–Tans method, the effective source $^{13}\text{C}/^{12}\text{C}$ ratio in the YRD was -24.37‰ , which was 0.21‰ higher than that in the Nanjing

Municipality. These results were consistent with inventory estimates of anthropogenic source ratios at these two spatial scales.

By combining inventory data on anthropogenic carbon sources and the atmospheric measurement of CO_2 mole fraction and $^{13}\text{C}/^{12}\text{C}$ ratio in an isotopic partitioning framework, we inferred that natural ecosystems in the YRD were a negligibly small source of atmospheric CO_2 , with an average flux of $(0.02 \pm 0.22)\text{ mg m}^{-2}\text{ s}^{-1}$ for 2014. In comparison, the CarbonTracker inverse analysis reveals a small annual mean daytime biological flux ($-0.01\text{ mg m}^{-2}\text{ s}^{-1}$) for this region for 2014.

6 Data availability

The atmospheric data are available upon request, as an electronic supplement to the paper or from the Yale–NUIST Center website <http://yncenter.sites.yale.edu>.

The Supplement related to this article is available online at doi:10.5194/acp-17-3385-2017-supplement.

Competing interests. The authors declare that they have no conflict of interest.

Acknowledgements. This research was supported by the National Natural Science Foundation of China (grant 41475141, 41505005), the US National Science Foundation (grant 1520684), the Ministry of Education of China (grant PCSIRT), and the Priority Academic Program Development of Jiangsu Higher Education Institutions (grant PAPD). The first author also acknowledges a visiting scholarship from China Scholarship Council and a Graduate Student Innovation grant from the Jiangsu Provincial Government (grant KYLX_0848). We thank the handling editor, Jan Kaiser, and four anonymous reviewers, whose constructive comments greatly improved this paper.

Edited by: J. Kaiser

Reviewed by: four anonymous referees

References

- Affek, H. P. and Eiler, J. M.: Abundance of mass 47- CO_2 in urban air, car exhaust, and human breath, *Geochim. Cosmochim. Ac.*, 70, 1–12, 2006.
- Akbari, H., Menon, S., and Rosenfeld, A.: Global cooling: increasing world-wide urban albedos to offset CO_2 , *Climatic Change*, 94, 275–286, 2009.
- An, H.: Ammonia synthesis: current status and future outlook, *Coal Chem. West. China*, 2, 4–13, 2012.
- Andres, R. J., Marland, G., Boden, T., and Bischof, S.: Carbon dioxide emissions from fossil fuel consumption and cement manufacture, 1751–1991; and an estimate of their isotopic composition and latitudinal distribution, Oak Ridge National Lab., TN, USA, 1994.

- Bai, Y.: A Comparative Study on Turbulent Fluxes Exchange over Nanjing Urban and Suburban in Summer, MS Thesis, Nanjing University of Information Science & Technology, Nanjing, 2011.
- Ballantyne, A. P., Miller, J. B., Baker, I. T., Tans, P. P., and White, J. W. C.: Novel applications of carbon isotopes in atmospheric CO_2 : what can atmospheric measurements teach us about processes in the biosphere?, *Biogeosciences*, 8, 3093–3106, doi:10.5194/bg-8-3093-2011, 2011.
- Ballantyne, A. P., Miller, J. B., and Tans, P. P.: Apparent seasonal cycle in isotopic discrimination of carbon in the atmosphere and biosphere due to vapor pressure deficit, *Global Biogeochem. Cy.*, 24, 1–16, 2010.
- Bi, J., Zhang, R., Wang, H., Liu, M., and Wu, Y.: The benchmarks of carbon emissions and policy implications for China's cities: Case of Nanjing, *Energy Policy*, 39, 4785–4794, 2011.
- Bowling, D. R., Sargent, S. D., Tanner, B. D., and Ehleringer, J. R.: Tunable diode laser absorption spectroscopy for stable isotope studies of ecosystem–atmosphere CO_2 exchange, *Agr. Forest Meteorol.*, 118, 1–19, 2003.
- Bowling, D. R., Burns, S. P., Conway, T. J., Monson, R. K., and White, J. W. C.: Extensive observations of CO_2 carbon isotope content in and above a high-elevation subalpine forest, *Global Biogeochem. Cy.*, 19, GB3023, doi:10.1029/2004GB002394, 2005.
- Bush, S. E., Pataki, D. E., and Ehleringer, J. R.: Sources of variation in $\delta^{13}\text{C}$ of fossil fuel emissions in Salt Lake City, USA, *Appl. Geochem.*, 22, 715–723, 2007.
- CESY: China Energy Statistical Yearbook 2013: China Statistical Publishing House, Beijing, also available at: <http://www.stats.gov.cn/tjsj/nds/2013/indexch.htm> (last access: 22 February 2016), 2013.
- China Cement: <http://hy.ccement.com/map/>, last access: 6 July 2016.
- Clark-Thorne, S. T. and Yapp, C. J.: Stable carbon isotope constraints on mixing and mass balance of CO_2 in an urban atmosphere: Dallas metropolitan area, Texas, USA, *Appl. Geochem.*, 18, 75–95, 2003.
- Coutts, A. M., Beringer, J., and Tapper, N. J.: Characteristics influencing the variability of urban CO_2 fluxes in Melbourne, Australia, *Atmos. Environ.*, 41, 51–62, 2007.
- CSY: China Statistical Yearbook, National Bureau of Statistics of China, also available at: <http://www.stats.gov.cn/tjsj/nds/2013/indexch.htm> (last access: 22 February 2016), 2013.
- Duan, Y.: Study of characteristics of coal isotope composition in China, *Coal Geol. Explor.*, 23, 29–33, 1995.
- Ehleringer, J. R., Bowling, D. R., Flanagan, L. B., Fessenden, J., Helliker, B., Martinelli, L. A., and Ometto, J. P.: Stable isotopes and carbon cycle processes in forests and grasslands, *Plant Biol.*, 4, 181–189, 2002.
- Farquhar, G. and Lloyd, J.: Carbon and oxygen isotope effects in the exchange of carbon dioxide between terrestrial plants and the atmosphere, *Stable Isotopes Plant Carb.-Water Relat.*, 40, 47–70, 1993.
- Fessenden, J. E. and Ehleringer, J. R.: Age-related variations in $\delta^{13}\text{C}$ of ecosystem respiration across a coniferous forest chronosequence in the Pacific Northwest, *Tree Physiol.*, 22, 159–167, 2002.
- Friedman, L. and Irsa, A. P.: Variations in isotopic composition of carbon in urban atmospheric carbon dioxide, *Science*, 158, 263–264, 1967.
- Gorski, G., Strong, C., Good, S. P., Bares, R., Ehleringer, J. R., and Bowen, G. J.: Vapor hydrogen and oxygen isotopes reflect water of combustion in the urban atmosphere, *P. Natl. Acad. Sci. USA*, 112, 3247–3252, 2015.
- Griffis, T. J.: Tracing the flow of carbon dioxide and water vapor between the biosphere and atmosphere: A review of optical isotope techniques and their application, *Agr. Forest Meteorol.*, 174, 85–109, 2013.
- Griffis, T. J., Lee, X., Baker, J. M., Sargent, S. D., and King, J. Y.: Feasibility of quantifying ecosystem–atmosphere $\text{C}^{18}\text{O}^{16}\text{O}$ exchange using laser spectroscopy and the flux-gradient method, *Agr. Forest Meteorol.*, 135, 44–60, 2005.
- Guha, T. and Ghosh, P.: Diurnal variation of atmospheric CO_2 concentration and $\delta^{13}\text{C}$ in an urban atmosphere during winter–role of the nocturnal boundary layer, *J. Atmos. Chem.*, 65, 1–12, 2010.
- Guha, T. and Ghosh, P.: Diurnal and seasonal variation of mixing ratio and $\delta^{13}\text{C}$ of air CO_2 observed at an urban station Bangalore, India, *Environ. Sci. Poll. Res.*, 22, 1877–1890, 2015.
- ICLEI – International Council for Local Environmental Initiatives: Local government operations protocol for the quantification and reporting of greenhouse gas emissions inventories, available at: <http://www.arb.ca.gov/cc/protocols/localgov/archive/finalgoproto2008-09-25.pdf> (last access: 18 August 2015), 2008.
- Jasechko, S., Gibson, J. J., and Edwards, T. W.: Stable isotope mass balance of the Laurentian Great Lakes, *J. Great Lakes Res.*, 40, 336–346, 2014.
- Jasek, A., Zimnoch, M., Gorczyca, Z., Smula, E., and Rozanski, K.: Seasonal variability of soil CO_2 flux and its carbon isotope composition in Krakow urban area, Southern Poland, *Isotopes Environ. Health Stud.*, 50, 143–155, 2014.
- Keeling, C. D.: The concentration and isotopic abundances of atmospheric carbon dioxide in rural areas, *Geochim. Cosmochim. Ac.*, 13, 322–334, 1958.
- Keeling, C. D.: The concentration and isotopic abundances of carbon dioxide in rural and marine air, *Geochim. Cosmochim. Ac.*, 24, 277–298, 1961.
- Koerner, B. and Klopatek, J.: Anthropogenic and natural CO_2 emission sources in an arid urban environment, *Environ. Pollut.*, 116, S45–S51, 2002.
- Leavitt, S. W., Paul, E. A., Galadima, A., Nakayama, F. S., Danzer, S. R., Johnson, H., and Kimball, B. A.: Carbon isotopes and carbon turnover in cotton and wheat FACE experiments, *Plant Soil*, 187, 147–155, 1995.
- Lee, X., Sargent, S., Smith, R., and Tanner, B.: In situ measurement of the water vapor $^{18}\text{O}/^{16}\text{O}$ isotope ratio for atmospheric and ecological applications, *J. Atmos. Ocean. Tech.*, 22, 555–565, 2005.
- Lichtfouse, E., Lichtfouse, M., and Jaffrezic, A.: $\delta^{13}\text{C}$ values of grasses as a novel indicator of pollution by fossil-fuel-derived greenhouse gas CO_2 in urban areas, *Environ. Sci. Technol.*, 37, 87–89, 2003.
- Liu, H. Z., Feng, J. W., Järvi, L., and Vesala, T.: Four-year (2006–2009) eddy covariance measurements of CO_2 flux over an urban area in Beijing, *Atmos. Chem. Phys.*, 12, 7881–7892, doi:10.5194/acp-12-7881-2012, 2012.

- Lloyd, J., Kruijt, B., Hollinger, D. Y., Grace, J., Francey, R. J., Wong, S., Kelliher, F. M., Miranda, A. C., Farquhar, G. D., and Gash, J. H. C.: Vegetation effects on the isotopic composition of atmospheric CO_2 at local and regional scales: theoretical aspects and a comparison between rain forest in Amazonia and a boreal forest in Siberia, *Funct. Plant Biol.*, 23, 371–399, 1996.
- Lloyd, J., Francey, R. J., Mollicone, D., Raupach, M. R., Sogachev, A., Arneeth, A., Byers, J. N., Kelliher, F. M., Rebmann, C., and Valentini, R.: Vertical profiles, boundary layer budgets, and regional flux estimates for CO_2 and its $^{13}\text{C}/^{12}\text{C}$ ratio and for water vapor above a forest/bog mosaic in central Siberia, *Global Biogeochem. Cy.*, 15, 267–284, 2001.
- McDonald, B. C., McBride, Z. C., Martin, E. W., and Harley, R. A.: High-resolution mapping of motor vehicle carbon dioxide emissions, *J. Geophys. Res.-Atmos.*, 119, 5283–5298, 2014.
- McManus, J. B., Zahniser, M. S., Nelson, D. D., Williams, L. R., and Kolb, C. E.: Infrared laser spectrometer with balanced absorption for measurement of isotopic ratios of carbon gases, *Spectrochim. Ac. Pt. A*, 58, 2465–2479, 2002.
- Miller, J. B. and Tans, P. P.: Calculating isotopic fractionation from atmospheric measurements at various scales, *Tellus B*, 55, 207–214, 2003.
- Miller, J. B., Tans, P. P., White, J. W. C., Conway, T. J., and Vaughn, B. W.: The atmospheric signal of terrestrial carbon isotopic discrimination and its implication for partitioning carbon fluxes, *Tellus B*, 55, 197–206, 2003.
- Moore, J. and Jacobson, A. D.: Seasonally varying contributions to urban CO_2 in the Chicago, Illinois, USA region: Insights from a high-resolution CO_2 concentration and $\delta^{13}\text{C}$ record, *Elementa*, 3, 000052, doi:10.12952/journal.elementa.000052, 2015.
- Mu, H., Li, H., Zhang, M., and Li, M.: Analysis of China's carbon dioxide flow for 2008, *Energy Policy*, 54, 320–326, 2013.
- Newman, S., Xu, X., Gurney, K. R., Hsu, Y. K., Li, K. F., Jiang, X., Keeling, R., Feng, S., O'Keefe, D., Patarasuk, R., Wong, K. W., Rao, P., Fischer, M. L., and Yung, Y. L.: Toward consistency between trends in bottom-up CO_2 emissions and top-down atmospheric measurements in the Los Angeles megacity, *Atmos. Chem. Phys.*, 16, 3843–3863, doi:10.5194/acp-16-3843-2016, 2016.
- Newman, S., Xu, X., Affek, H. P., Stolper, E., and Epstein, S.: Changes in mixing ratio and isotopic composition of CO_2 in urban air from the Los Angeles basin, California, between 1972 and 2003, *J. Geophys. Res.*, 113, 1–15, 2008.
- NSY: Nanjing Statistical Yearbook, Nanjing Municipal Bureau Statistics, also available at: <http://www.njtj.gov.cn/2004/2013/renmin/index.htm> (last access: 22 February 2016), 2003.
- Ometto, J. P., Flanagan, L. B., Martinelli, L. A., Moreira, M. Z., Higuchi, N., and Ehleringer, J. R.: Carbon isotope discrimination in forest and pasture ecosystems of the Amazon Basin, Brazil, *Global Biogeochem. Cy.*, 16, 1–10, 2002.
- Ometto, J. P., Ehleringer, J. R., Domingues, T. F., Berry, J. A., Ishida, F. Y., Mazzi, E., Higuchi, N., Flanagan, L. B., Nardoto, G. B., and Martinelli, L. A.: The stable carbon and nitrogen isotopic composition of vegetation in tropical forests of the Amazon Basin, Brazil, *Biogeochemistry*, 79, 251–274, 2006.
- Pan, J.: Theoretical and Process Studies of the Abatement of Fuel Gas Emissions during Iron Ore Sintering, PhD Dissertation, Southcentral University of China, Changsha, Hunan Province, 2007.
- Pang, J., Wen, X., and Sun, X.: Mixing ratio and carbon isotopic composition investigation of atmospheric CO_2 in Beijing, China, *Sci. Total Environ.*, 539, 322–330, 2016.
- Pataki, D. E., Bowling, D. R., and Ehleringer, J. R.: Seasonal cycle of carbon dioxide and its isotopic composition in an urban atmosphere: Anthropogenic and biogenic effects, *J. Geophys. Res.-Atmos.*, 108, 1–8, 2003a.
- Pataki, D. E., Ehleringer, J. R., Flanagan, L. B., Yakir, D., Bowling, D. R., Still, C. J., Buchmann, N., Kaplan, J. O., and Berry, J. A.: The application and interpretation of Keeling plots in terrestrial carbon cycle research, *Global Biogeochem. Cy.*, 17, 1–14, 2003b.
- Pataki, D. E., Bowling, D. R., Ehleringer, J. R., and Zobitz, J. M.: High resolution atmospheric monitoring of urban carbon dioxide sources, *Geophys. Res. Lett.*, 33, 1–5, 2006.
- Pataki, D. E., Lai, C., Keeling, C. D., and Ehleringer, J. R.: Insights from stable isotopes on the role of terrestrial ecosystems in the global carbon cycle, in: *Terrestrial Ecosystems in a Changing World*, Springer, Berlin, Germany, 37–44, 2007.
- Pataki, D. E., Emmi, P. C., Forster, C. B., Mills, J. I., Pardyjak, E. R., Peterson, T. R., Thompson, J. D., and Dudley-Murphy, E.: An integrated approach to improving fossil fuel emissions scenarios with urban ecosystem studies, *Ecol. Complex.*, 6, 1–14, 2009.
- Peters, W., Jacobson, A. R., Sweeney, C., Andrews, A. E., Conway, T. J., Masarie, K., Miller, J. B., Bruhwiler, L. M., Petron, G., Hirsch, A. I., Worthy, D. E., van der Werf, G. R., Randerson, J. T., Wennberg, P. O., Krol, M. C., and Tans, P. P.: An atmospheric perspective on North American carbon dioxide exchange: CarbonTracker, *P. Natl. Acad. Sci. USA*, 104, 18925–18930, 2007.
- Prairie, Y. T. and Duarte, C. M.: Direct and indirect metabolic CO_2 release by humanity, *Biogeosciences*, 4, 215–217, doi:10.5194/bg-4-215-2007, 2007.
- Rella, C.: Accurate stable carbon isotope ratio measurements with rapidly varying carbon dioxide concentrations using the Picarro $\delta^{13}\text{C}$ G2101-i gas analyzer, Picarro White Paper, Picarro Inc., Sunnyvale, California, 2011.
- Ren, L., Wang, W., Wang, J., and Liu, R.: Analysis of energy consumption and carbon emission during the urbanization of Shandong Province, China, *J. Clean. Prod.*, 103, 534–541, 2015.
- Röckmann, T., Eyer, S., van der Veen, C., Popa, M. E., Tuzson, B., Monteil, G., Houweling, S., Harris, E., Brunner, D., Fischer, H., Zazzeri, G., Lowry, D., Nisbet, E. G., Brand, W. A., Necki, J. M., Emmenegger, L., and Mohn, J.: In situ observations of the isotopic composition of methane at the Cabauw tall tower site, *Atmos. Chem. Phys.*, 16, 10469–10487, doi:10.5194/acp-16-10469-2016, 2016.
- Rose, L. S., Akbari, H., and Taha, H.: Characterizing the fabric of the urban environment: a case study of Greater Houston, Texas, National Laboratory, Lawrence, Berkeley, 2003.
- Satterthwaite, D.: Cities' contribution to global warming: notes on the allocation of greenhouse gas emissions, *Environ. Urban.*, 20, 539–549, 2008.
- Shen, S., Yang, D., Xiao, W., Liu, S., and Lee, X.: Constraining anthropogenic CH_4 emissions in Nanjing and the Yangtze River Delta, China, using atmospheric CO_2 and CH_4 mixing ratios, *Adv. Atmos. Sci.*, 31, 1343–1352, 2014.
- Song, T. and Wang, Y.: Carbon dioxide fluxes from an urban area in Beijing, *Atmos. Res.*, 106, 139–149, 2012.
- Sturm, P., Leuenberger, M., Valentino, F. L., Lehmann, B., and Ihly, B.: Measurements of CO_2 , its stable isotopes, O_2/N_2 , and

- ^{222}Rn at Bern, Switzerland, *Atmos. Chem. Phys.*, 6, 1991–2004, doi:10.5194/acp-6-1991-2006, 2006.
- Sun, B., Dilcher, D. L., Beerling, D. J., Zhang, C., Yan, D., and Kowalski, E.: Variation in Ginkgo biloba L. leaf characters across a climatic gradient in China, *P. Natl. Acad. Sci. USA*, 100, 7141–7146, 2003.
- Takahashi, H. A., Konohira, E., Hiyama, T., Minami, M., Nakamura, T., and Yoshida, N.: Diurnal variation of CO_2 concentration, $\delta^{14}\text{C}$ and $\delta^{13}\text{C}$ in an urban forest: estimate of the anthropogenic and biogenic CO_2 contributions, *Tellus B*, 54, 97–109, 2002.
- Thoning, K. W., Tans, P. P., and Komhyr, W. D.: Atmospheric carbon dioxide at Mauna Loa Observatory: 2. Analysis of the NOAA GMCC data, 1974–1985, *J. Geophys. Res.*, 94, 8549–8565, 1989.
- Vardag, S. N., Hammer, S., and Levin, I.: Evaluation of 4 years of continuous $\delta^{13}\text{C}(\text{CO}_2)$ data using a moving Keeling plot method, *Biogeosciences*, 13, 4237–4251, doi:10.5194/bg-13-4237-2016, 2016.
- Wada, R., Nakayama, T., Matsumi, Y., Hiyama, T., Inoue, G., and Shibata, T.: Observation of carbon and oxygen isotopic compositions of CO_2 at an urban site in Nagoya using Mid-IR laser absorption spectroscopy, *Atmos. Environ.*, 45, 1168–1174, 2011.
- Wang, D.: Method and Empirical Research of Urban Greenhouse Gas Measurement, MS Thesis, Tianjin University, Tianjin, 2013.
- Wang, W. and Pataki, D. E.: Drivers of spatial variability in urban plant and soil isotopic composition in the Los Angeles basin, *Plant Soil*, 350, 323–338, 2012.
- Wehr, R. and Saleska, S. R.: The long-solved problem of the best-fit straight line: application to isotopic mixing lines, *Biogeosciences*, 14, 17–29, doi:10.5194/bg-14-17-2017, 2017.
- Wen, X.-F., Meng, Y., Zhang, X.-Y., Sun, X.-M., and Lee, X.: Evaluating calibration strategies for isotope ratio infrared spectroscopy for atmospheric $^{13}\text{CO}_2/^{12}\text{CO}_2$ measurement, *Atmos. Meas. Tech.*, 6, 1491–1501, doi:10.5194/amt-6-1491-2013, 2013.
- Widory, D.: Combustibles, fuels and their combustion products: A view through carbon isotopes, *Combust. Theory Model.*, 10, 831–841, 2006.
- Widory, D. and Javoy, M.: The carbon isotope composition of atmospheric CO_2 in Paris, *Earth Planet. Sc. Lett.*, 215, 289–298, 2003.
- Yakir, D. and da Sternberg, L.: The use of stable isotopes to study ecosystem gas exchange, *Oecologia*, 123, 297–311, 2000.
- Yang, H. M., Wang, H. Z., and Wu, Y. B.: Observation and characteristics analysis of traffic flow in Nanjing, *Environ. Sci. Technol.*, 24, 98–101, 2011.
- Zhou, L., Conway, T. J., White, J. W., Mukai, H., Zhang, X., Wen, Y., Li, J., and MacClune, K.: Long-term record of atmospheric CO_2 and stable isotopic ratios at Waliguan Observatory: Background features and possible drivers, 1991–2002, *Global Biogeochem. Cy.*, 19, GB3021, doi:10.1029/2004GB002430, 2005.
- Zimnoch, M., Florkowski, T., Necki, J. M., and Neubert, R. E.: Diurnal variability of $\delta^{13}\text{C}$ and $\delta^{18}\text{O}$ of atmospheric CO_2 in the urban atmosphere of Kraków, Poland, *Isotopes Environ. Health Stud.*, 40, 129–143, 2004.
- Zobitz, J. M., Burns, S. P., Reichstein, M., and Bowling, D. R.: Partitioning net ecosystem carbon exchange and the carbon isotopic disequilibrium in a subalpine forest, *Global Change Biol.*, 14, 1785–1800, 2008.
- Zondervan, A. and Meijer, H. A.: Isotopic characterisation of CO_2 sources during regional pollution events using isotopic and radiocarbon analysis, *Tellus B*, 48, 601–612, 1996.